JGR Atmospheres

RESEARCH ARTICLE
10.1029/2020JD034196

Atmospheric Rivers Impacting Northern California Exhibit a Quasi-Decadal Frequency

Jacob Stuivenvolt-Allen[1], Shih-Yu Simon Wang[1,2], Zachary Johnson[1], and Yoshimitsu Chikamoto[1]

[1]Department of Plants, Soils, and Climate, Utah State University, Logan, UT, USA, [2]IBPA, College of Agriculture and Natural Resources, National Chung Hsing University, Taichung, Taiwan

Key Points:

- The frequency of atmospheric rivers over Northern California exhibits a pronounced quasi-decadal cycle
- Cyclical variability in the tropical Pacific accentuates or weakens the Aleutian Low–impacting atmospheric river frequency
- This analysis provides metrics for improving decadal prediction of atmospheric rivers and regional surface hydrology

Supporting Information:

Supporting Information may be found in the online version of this article.

Correspondence to:

J. Stuivenvolt-Allen,
jacob.stuivenvoltallen@usu.edu

Citation:

Stuivenvolt-Allen, J., Wang, S.-Y. S., Johnson, Z., & Chikamoto, Y. (2021). Atmospheric rivers impacting Northern California exhibit a quasi-decadal frequency. *Journal of Geophysical Research: Atmospheres*, *126*, e2020JD034196. https://doi.org/10.1029/2020JD034196

Received 5 NOV 2020
Accepted 16 JUL 2021

Author Contributions:

Conceptualization: Jacob Stuivenvolt-Allen, Shih-Yu Simon Wang, Yoshimitsu Chikamoto
Data curation: Jacob Stuivenvolt-Allen, Zachary Johnson, Yoshimitsu Chikamoto
Formal analysis: Jacob Stuivenvolt-Allen
Funding acquisition: Shih-Yu Simon Wang
Investigation: Jacob Stuivenvolt-Allen
Methodology: Jacob Stuivenvolt-Allen, Shih-Yu Simon Wang, Zachary Johnson, Yoshimitsu Chikamoto
Project Administration: Shih-Yu Simon Wang
Resources: Shih-Yu Simon Wang
Software: Jacob Stuivenvolt-Allen
Supervision: Shih-Yu Simon Wang, Yoshimitsu Chikamoto

Abstract Periods of water surplus and deficit in Northern California follow a pronounced quasi-decadal cycle. This cycle is largely driven by the frequency of atmospheric rivers (ARs), affecting the region's wet and dry periods. Our analyses demonstrate that the quasi-decadal cycle of AR frequency relies on moisture transport associated with the position and intensity of the Aleutian Low. In observations, the Aleutian Low is shown to covary with tropical Pacific sea surface temperature anomalies. A modeling experiment, which incorporates ocean observations from the equatorial Pacific into the fully coupled climate model, provides support that the quasi-decadal cycle of the Aleutian Low is forced by the tropical Pacific. Subsequently, the tropical Pacific modulates the wet season moisture transport toward California on decadal time scales, affecting AR frequency. These results provide metrics for improving interannual-to-decadal prediction of AR activity, which drives hydrological cycles in Northern California.

Plain Language Summary In Northern California, much of the precipitation and surface water comes from atmospheric rivers–corridors of moisture transport from the tropics. The frequency of atmospheric rivers is cyclical, with periods of water surplus and deficit in the region that repeat every 10–17 years. While many social and political factors influence water resource distribution, understanding the climate factors that regulate water availability is important for managing water in the future. Using data from observations and modeling experiments, the pronounced wet/dry cycle in this area of the Western United States is mainly attributed to regular fluctuations in sea surface temperatures in the tropical Pacific Ocean. This analysis provides a potential source of predictability for atmospheric river frequency, and thus water availability, years before a winter season.

1. Introduction

Water resources along the Pacific Coast of the United States are closely tied to the frequency and magnitude of cold-season precipitation associated with atmospheric rivers (ARs) (M. Dettinger, 2011). ARs transport large amounts of moisture from the tropics to the poles and have been studied extensively on seasonal to annual timescales for their "drought busting" characteristics and potential flooding hazards (M. D. Dettinger, 2013; Gershunov et al., 2017; Guan et al., 2010). While the seasonal to annual variability is important for surface hydrology a recent study in the Emerald Triangle region of Northern California (Trinity, Mendocino, and Humboldt counties, Figure 1a) showed that longer scales, within a 10- to 17-year range, are the most prominent feature in the region's surface and atmospheric moisture, stimulating interest in understanding the source of this cycle (Morgan et al., 2020). Dettinger and Cayan (2014) have also documented pronounced 15-year variability in ARs and precipitaiton for the California Delta, highlighting that low-frequency variability is likely an integral part of the region's water cycle (Dettinger, 2016). These low-frequency cycles are referred to as quasi-decadal owing to their almost 10-year period. While the quasi-decadal cycle in atmospheric and surface moisture was prominent in this sub-region of Northern California, one objective of this research is to determine if the quasi-decadal cycle is a common feature for the rest of Northern California (the area used for tracking the coastal entry of Northern California ARs is shown in the black box on Figure 1b along with topography). Additionally, because low-frequency atmospheric variability is largely affected by ocean variability, our other objective is to evaluate the ocean's role in influencing this quasi-decadal cycle and identify which component of the climate system maintains the quasi-decadal variability in ARs.

Validation: Jacob Stuivenvolt-Allen
Visualization: Jacob Stuivenvolt-Allen
Writing – original draft: Jacob Stuivenvolt-Allen, Yoshimitsu Chikamoto
Writing – review & editing: Jacob Stuivenvolt-Allen, Shih-Yu Simon Wang, Zachary Johnson, Yoshimitsu Chikamoto

With a few exceptions (Dettinger & Cayan, 2014; Gershunov et al., 2017; Guirguis et al., 2019), AR literature focuses on relatively short time scales. This can largely be explained by the short history of high-resolution climate data to analyze the frequency and characteristics of ARs and regional precipitation. These studies have highlighted three patterns of extra-tropical atmospheric circulation that affect interannual cycles of AR frequency during the wet season (November through March; Figure 1c): The Pacific North American (PNA) pattern, the North Pacific Oscillation (NPO), and the North American Winter Dipole (NAWD). These seasonal climate patterns can oscillate between positive and negative phases, in which the location of the pressure anomalies is maintained, but the sign of the pressure anomaly is reversed. The negative phase of the PNA pattern has been associated with enhanced AR activity in the Pacific Northwest, due to the negative pressure anomaly just offshore of the western U.S. (Guan et al., 2013; Guan & Waliser, 2015; Mundhenk et al., 2018). The NPO, characterized by a meridional pressure seesaw in the North Pacific, enhances moisture transport toward the central Pacific Coast (encompassing the Emerald Triangle region) during its negative phase (Tan et al., 2020). The last notable pattern is the NAWD, with a positive phase that is characterized by an amplified ridge over western North America and an amplified trough over the eastern part of the continent during the boreal winter (Wang et al., 2015). The NAWD strongly influences California's precipitation variability (O'Brien et al., 2019; Wang et al., 2017), but has not been studied directly with ARs and has not been studied for any cyclical behavior. Due to their known relationship with northern California precipitation and ARs, these extratropical patterns are analyzed as potential contributors to the quasi-decadal cycle.

Atmospheric oscillations over long periods are heavily influenced by ocean variability (Patricola et al., 2020). Many previous studies point out that the El Niño Southern Oscillation (ENSO) impacts AR orientation, frequency, and intensity on interannual timescales (Bao et al., 2006; Guirguis et al., 2019; Higgins et al., 2000; Payne & Magnusdottir, 2014; Ryoo et al., 2013). On longer timescales, however, there is still uncertainty about the role of decadal ENSO or ENSO flavor (Timmermann et al., 2018) and how it affects AR activity (Guirguis et al., 2019; Kim & Alexander, 2015). While the positive Pacific Decadal Oscillation (PDO) enhances AR activity for the Northeastern Pacific (Gershunov et al., 2017; Liu et al., 2016), its dominant cycle of 30–50 years (MacDonald & Case, 2005; Newman et al., 2016) does not compare with the quasi-decadal cycle in AR frequency over the Emerald Triangle. The last pattern of ocean variability we analyze is the North Pacific Gyre Oscillation (NPGO) which modulates water vapor transport to western North America and is characterized by strong decadal variability (Liu et al., 2016; Lorenzo et al., 2008).

To evaluate the quasi-decadal cycle in ARs, it is important to have data with sufficient length to account for the reduction in degrees of freedom when looking at decadal variability. Additionally, tracking ARs requires data with a sufficient representation of tropospheric moisture and winds to capture the features and frequency of ARs. To satisfy these requirements, we adapted an AR tracking method from Gershunov et al. (2017) and produced a frequency record of ARs reaching coastal Northern California that spans more than seven decades. While a longer record of ARs is desirable, the lack of observational data before the mid-twentieth century reduces the reliability of atmospheric moisture and wind data in reanalysis (Hersbach et al., 2015; Slivinski et al., 2019).

To identify the ocean and atmosphere's influence on the quasi-decadal cycle, we evaluate the contributions of atmospheric teleconnection patterns and ocean variability in the Pacific toward AR frequency during the wet season (November through the following March). These months account for more than 80% of the region's annual precipitation and are the most common months for landfalling ARs (Figure 1c) (Guirguis et al., 2019). First, we show the relationship between ARs and the ocean in observations. To validate the results of observations and provide potential primary forcing mechanisms, we make use of a climate modeling experiment with the fully coupled Community Earth System Model (CESM). Literature focused on decadal variability and impacts to extra-tropical atmospheric circulation in the north Pacific has often highlighted the tropical Pacific as a primary forcing (Di Lorenzo et al., 2010; Johnson et al., 2020; Rodgers et al., 2004; L. Wu et al., 2003). In particular, decadal components of ENSO variability have shown a strong relationship with precipitation and temperature variability in western North America (George & Ault, 2011; Wang et al., 2011). Through a three-dimensional assimilation of observed sea surface temperatures and salinity from the tropical Pacific alone, the CESM allows us to evaluate the role of the tropical Pacific in the quasi-decadal cycle and discuss the important climate features for modulating low-frequency variability in ARs for the entire Northern California region.

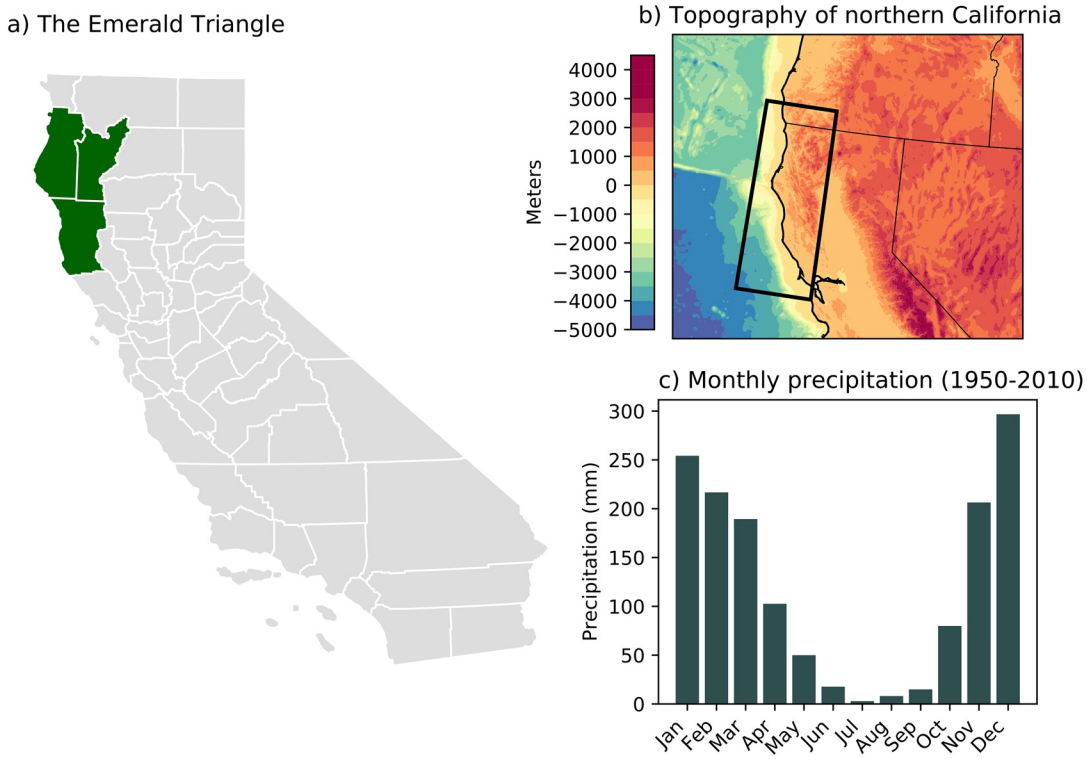

Figure 1. (a) County map of California with the Emerald Triangle (Humboldt, Mendocino, and Trinity counties) shown in green. (b) Topographic map of Northern California with the black box indicating the area used for atmospheric river (AR) tracking. (c) Histogram of monthly precipitation from 1950 through 2020 in the boxed region from panel b.

2. Data and Methods and Model Experiment

2.1. Observational Data

Monthly precipitation (1890–2019) and soil moisture data (1948–2019) at 1° resolution were provided by the Global Precipitation Climatology Project Centre version 6.0 (Schneider et al., 2014) and the NOAA Climate Prediction Center (Fan & Van Den Dool, 2004), respectively. Streamflow data comprising the standardized average of 11 gauges within the Emerald Triangle with consistent records for at least 65 years in the United States Geological Survey (Morgan et al., 2020). Available climate indices (PNA, NPO, Niño 1 + 2, Niño 4, PDO, and NPGO) were obtained from the NOAA Physical Science Laboratory (https://psl.noaa.gov/). The NAWD index was calculated following Wang et al. (2014) by subtracting the area average of 300 hPa geopotential height anomalies at the center of the ridge location (132.5°–137.5°W and 47.5°–52.5°N) from the 300 hPa geopotential height anomalies at the eastern trough center (77.5°–82.5°W and 57.5°–62.5°N). The monthly sea surface temperature (SST) data spanning 1948 to 2019 was provided by the Japanese Meteorological Agency's Centennial In-Situ Observation Based Estimates (COBE) SST at 1° resolution (Ishii et al., 2005). Monthly and 6-hourly three-dimensional atmospheric variables, such as geopotential height (GPH), specific humidity, and horizontal winds come from the National Center for Environmental Prediction's Reanalysis (NCEP R1) from 1948 to 2019 (Kalnay et al., 1996). Results in NCEP R1 are compared with the Japanese Meteorological Agency's reanalysis (JRA-55) at 1.25° x 1.25° resolution (Ebita et al., 2011). The wet season is defined as the average from November through the following March with the year corresponding to the year during January. All observational data are processed as anomalies from the 1981–2010 climatology with the linear trend removed to minimize any climate change signal.

2.2. AR Tracking

Slight changes in tracking methodology and the definitions of an AR can result in different frequencies and characteristics from automated AR detection (Rutz et al., 2019). To account for this, and produce a reliable

and long-term index of ARs over northern California (125°–122.5°W and 37.5°–42.5°N), we adapted a tracking algorithm from Gershunov et al. (2017) with insight from Rutz et al. (2019) to be used in the NCEP R1 at 6-h intervals. AR detection was based off of absolute thresholds, which is the recommended form of tracking for analyzing the relationship between ARs and large-scale atmospheric patterns (Rutz et al., 2019). These thresholds require minimum values of integrated vapor transport (IVT) at 250 $kg^1\ m^{-1}\ s^{-1}$ and total columnar integrated water vapor (IWV) at 15 mm. These thresholds filter out the background state and highlight anomalously high values of IVT and IWV that are uncommonly seen without AR conditions. IVT and IWV computations require the zonal and meridional components of wind at pressure levels from 1000 to 300 hPa, specific humidity, and surface pressure. To ensure that the threshold values over Northern California are part of a larger corridor of enhanced vapor transport, counting an AR also requires a length requirement in threshold values of IVT and IWV. Geometric requirements for AR detection were limited to the length of the event, requiring at least 2500 km of continuous threshold conditions of IVT and IWV. These threshold conditions were evaluated at the Northern Californian coast as the entry point for landfalling ARs in the region and then their characteristics were traced back, grid point by grid point until IVT and IWV conditions were not met.

NCEP R1 has been shown to have biases in atmospheric vapor transport, but the temporal variability of atmospheric vapor transport is accurate for well-observed regions (Gutowski et al., 1997). To ensure AR tracking in NCEP R1 is accurate, we compared results from our tracking with results from the Atmospheric River Intercomparison Project's (ARTMIP) published Tier One Catalog for the same region and season (Shields et al., 2018). These ARTMIP tracking routines were performed in the Modern-Era Retrospective analysis for Research and Applications 2 (MERRA) reanalysis data at 0.5° x 0.625° resolution, providing a test of how well the relatively coarse resolution of NCEP R1 can replicate annual frequency characteristics of ARs. While the NCEP R1 tracking was done over six-hour intervals, ARTMIP tracking was done over 3-h intervals. To account for this discrepancy, we used the ARTMIP algorithms which required a minimum time (12–18 h) for threshold values of IVT or IWV (or both) to classify an AR. In Figure S1, highly coherent interannual variability is found between the developed tracking algorithm and the results from ARTMIP's Tier One Catalog ($r = 0.80$ for the overlap period from 1980 to 2017). The annual AR frequency magnitudes vary significantly between NCEP R1 and the ARTMIP mean, which is unsurprising as there are similar differences in AR frequency magnitude between different algorithms within ARTMIP as well (Shields et al., 2018). To provide a second layer of verification that extends beyond the satellite era, the wet-season frequency of ARs was correlated with soil moisture, and precipitation for the tracking region (125°–122.5°W and 37.5°–42.5°N) and streamflow from the Emerald Triangle. A strong relationship between AR frequency, surface moisture, and precipitation shows that the AR frequency time series is physically meaningful for wet-season hydrology (Figure S2). Disparities in AR characteristics from tracking have been explored in other research (Shields et al., 2018) while this project is focused on interannual-to-decadal variability in frequency.

2.3. A Climate Modeling Experiment

Observational data is a useful tool for evaluating the relationships between the ocean and atmosphere—but modeling experiments can be particularly helpful for identifying the primary forcing mechanisms. Numerous studies have found the tropical Pacific Ocean to be the source of decadal variability (Di Lorenzo et al., 2010; Rodgers et al., 2004; S. Wu et al., 2011)—stimulating interest in isolating the impacts of this region. To evaluate the ocean's response in modulating interannual to quasi-decadal variability in Northern Californian Ars, this study examines experiments conducted by NCAR's fully coupled CESM version 1.0. The CESM consists of ocean, atmospheric, land, and sea-ice components with 26 atmospheric levels and 60 vertical levels in the ocean. The ocean and sea-ice components comprise a curvature horizontal grid with approximately 1° latitude and 3° longitude resolution at the equator but lower at higher latitudes. The atmosphere and land components have a T31 spectral grid (~3.75° resolution). Details of the model performance and settings can be found in Shields et al. (2012) and Chikamoto et al. (2015).

We ran a global ocean assimilation (GLOB run) and a historical assimilation comprising 10 ensemble members from initial conditions compiled from 10 random years in pre-industrial control simulations from 1958 to 2014. The historical simulation corresponds to the externally forced component from anthropogenic forc-

ing. In the GLOB run, we prescribed the same radiative forcing as the historical run and assimilate 3-dimensional observed temperature and salinity anomalies into the ocean component of the model while the atmosphere is free to evolve from ocean forcing. The assimilated observed ocean data originates from the ECMWF ocean reanalysis product (version 4) from 1958 to 2014 (Balmaseda et al., 2013), which is linearly interpolated from monthly to daily anomalies and added as forcing into the model's temperature and salinity tendency equations. To identify the equatorial Pacific's contribution to AR frequency, we further conduct a partial ocean assimilation using the same model configurations while assimilating the 3-dimensional observed salinity and temperature anomalies solely in the equatorial Pacific (10°S–10°N), with a buffering zone on the northern and southern boundaries of the assimilated domain. By only assimilating the equatorial Pacific Ocean information, namely the eqPAC run, the ocean and atmosphere components of CESM are free to evolve from equatorial Pacific forcing. Applications of the eqPAC method have been documented in previous studies (Chikamoto et al., 2016; Chikamoto, Wang, et al., 2020; Johnson et al., 2018, 2020; Purich et al., 2016).

All model data presented in this study consists of the average from November through the following March. Anomalies in this study are defined as deviations from the climatological mean for 1981–2010, a range chosen because it was the most recent climate normal at the time of this writing, in reanalysis and the model run (World Meteorological Organization, 2017). To remove any climate change signal, linear trends are removed from all data.

2.4. Power Spectra and Bandpass Filtering

To isolate the temporal scales that are important for Northern California ARs, power spectra analysis is used to show which periods explain the most variance in relevant moisture variables. Each time series is linearly detrended and normalized before computing the power spectra, which uses Fourier analysis to determine which frequencies contribute the most variance to the time series. This analysis (Figure 2) shows that the most prominent peak in the power spectra is 10–17 years for AR frequency, soil moisture, streamflow, and precipitation. Subsequently, we evaluate the relationship between unfiltered AR frequency and unfiltered climate variables (SST, 500 hPa GPH and IVT) which includes the total time-series variance and all scales of variability. To isolate the signal from the quasi-decadal cycle in ARs, we apply a bandpass filter which removes the variance not contributed by the 7- to 20-year oscillations. This window of time helps remove the influence of higher frequency ENSO variability (~4–6 years) along with lower frequency inter-decadal variability associated with the Interdecadal Pacific Oscillation (D'Arrigo et al., 2005; Mantua et al., 1997).

3. Observational Data Analysis

To help validate the tracking of ARs before the satellite era, correlations between AR frequency, and streamflow, precipitation and soil moisture for the Emerald Triangle are shown in Figure S2. Strong correlations between these variables and AR frequency indicate that the AR tracking before the satellite-era data provides physically meaningful AR metrics despite the stated shortcomings in NCEP R1. These results are consistent in both the unfiltered and the 7- to 20-year bandpass filtered data, supporting other studies highlighting pronounced decadal variability for Northern California (George & Ault, 2011; Wang et al., 2009). The power spectra analysis confirms these quasi-decadal cycles contribute significantly to the total variance of these hydrological variables, with spectral peaks at frequencies from about 10–17 years (Figure 2). Streamflow also exhibits a significant 4-year cycle although there are no such spectral peaks for the other hydrological variables (Figure 2). The 2-year spectral peak has been documented in western US hydrology and is likely related to the Biennial Annular Mode Oscillation (Johnstone, 2011). We focus on the quasi-decadal cycle because it is found in all moisture metrics for the region.

To examine the large-scale climate variability associated with the AR frequency, we made regression maps of 500 hPa geopotential height (Z500), IVT, and SST anomalies with AR frequency. Due to the stated deficiencies in NCEP R1, a comparison is also made with JRA-55 which yields analogous results when compared to Figure 3 (Figure S4). Two years before peaks of AR frequency, the regressions depict a north-south dipole of Z500 anomalies in the North Pacific, which resemble the NPO structure (Figure 3a). However, the moisture transport associated with NPO does not yet reach into Northern California (Figure 3b). At 1-year lead

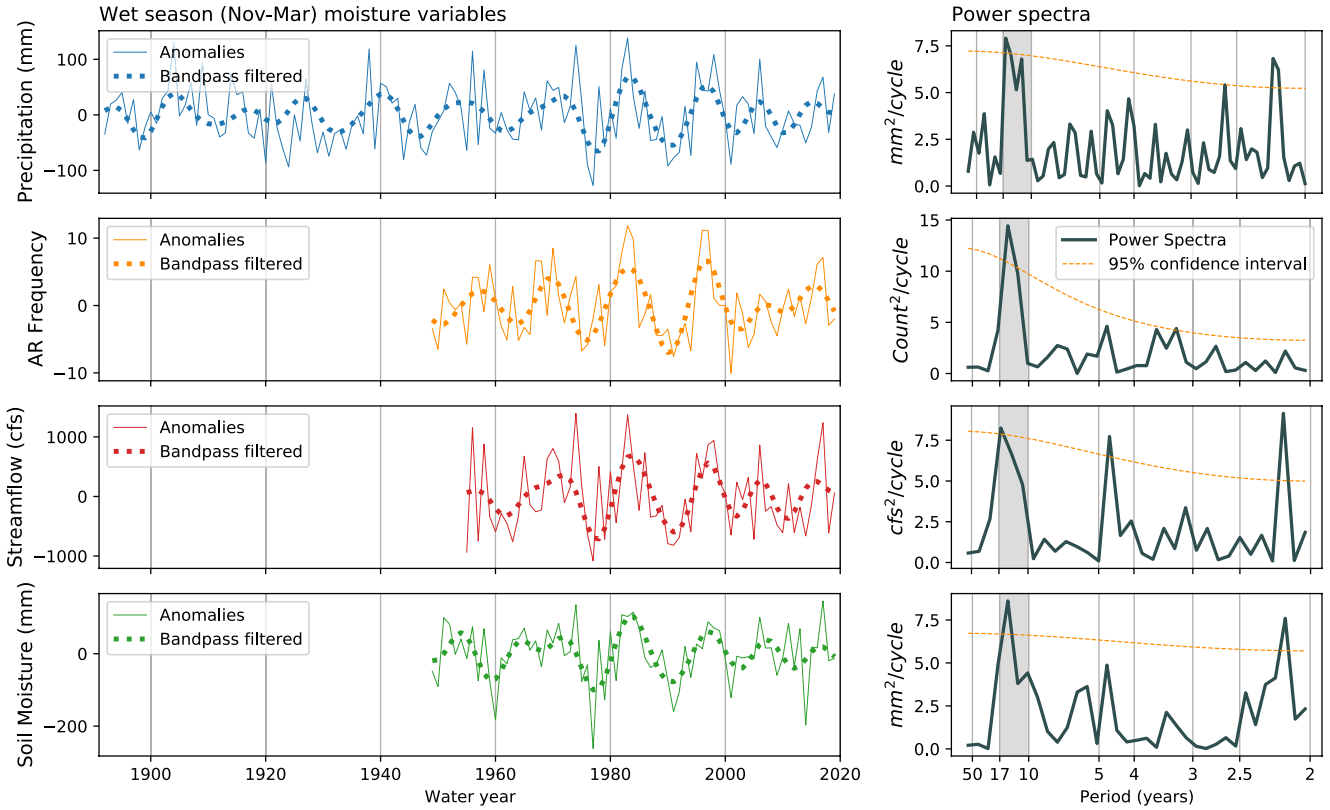

Figure 2. (Left column) Anomalies of precipitation, atmospheric river (AR) frequency, streamflow, and soil moisture along with the bandpass filtered time series. (Right column) Power spectra of the respective moisture variables with the 95% confidence interval represented by the power spectra of a first order Markov process. The gray shaded rectangle highlights the period of interest, the quasi-decadal frequency, from 10 to 17 years.

time, the negative Z500 anomaly is closer to the West Coast of North America (Figure 3d), enhancing the moisture transport toward Northern California (Figure 3e). The concurring regressions show the persistence of the negative Z500 anomaly in the northeast Pacific, with enhanced IVT over Northern California (Figures 3g and 3h). Broad areas of tropical Pacific SST anomalies exhibit a significant relationship with AR frequency at a 1- to 0-year lead time (Figures 3f and 3i), but the main forcing for the quasi-decadal variability of ARs is still unclear. Regressions of observed and unfiltered Z500 and IVT with streamflow (Figure S3) depict features of the NAWD and the PNA pattern. The El Niño-like pattern in year-1 (Figure 3f) suggests that Northern California's hydroclimate variability is coupled with the ENSO transition phase rather than the peak ENSO phase (Wang et al., 2014).

When we apply a 7- to 20-year bandpass filter to all anomalies, a clear evolution can be found in Z500, IVT, and SST. Tropical SST cooling at a 6-year lead results in an anti-cyclonic circulation anomaly over the northeast Pacific, inhibiting moisture transport into the region (Figures 4a–4c). Positive SST anomalies in the west-tropical Pacific appear around the 3-year lead and the extra-tropical atmosphere facilitates more moisture transport to Southern California through the cyclonic circulation anomaly around the latitude band of 20°–40°N (Figures 4d–4f). The concurrent regressions feature a deepened Aleutian Low (Figure 4g), enhanced tropical moisture transport (Figure 4h), and a broad area of tropical SST warming. The central Pacific is the main contributor to the maintenance of decadal variability for much of the Pacific basin (Deser et al., 2011; Knutson & Manabe, 1998; Yeh & Kirtman, 2005), but our results highlight that peak AR activity does not occur in tandem with central Pacific warming (Figure 4f). Instead, the ENSO impact on the hydroclimate of Northern California is delayed for about a year after the peak of the event (Figure 4i).

To further isolate climate variability with similar low-frequency oscillations to ARs, we applied power spectra to the teleconnection indices of interest. In the atmosphere, the NPO and the NAWD exhibit a pronounced 10- to 17-year periodicity. The PNA dominates on timescales around 3–4 years and 5–6 years,

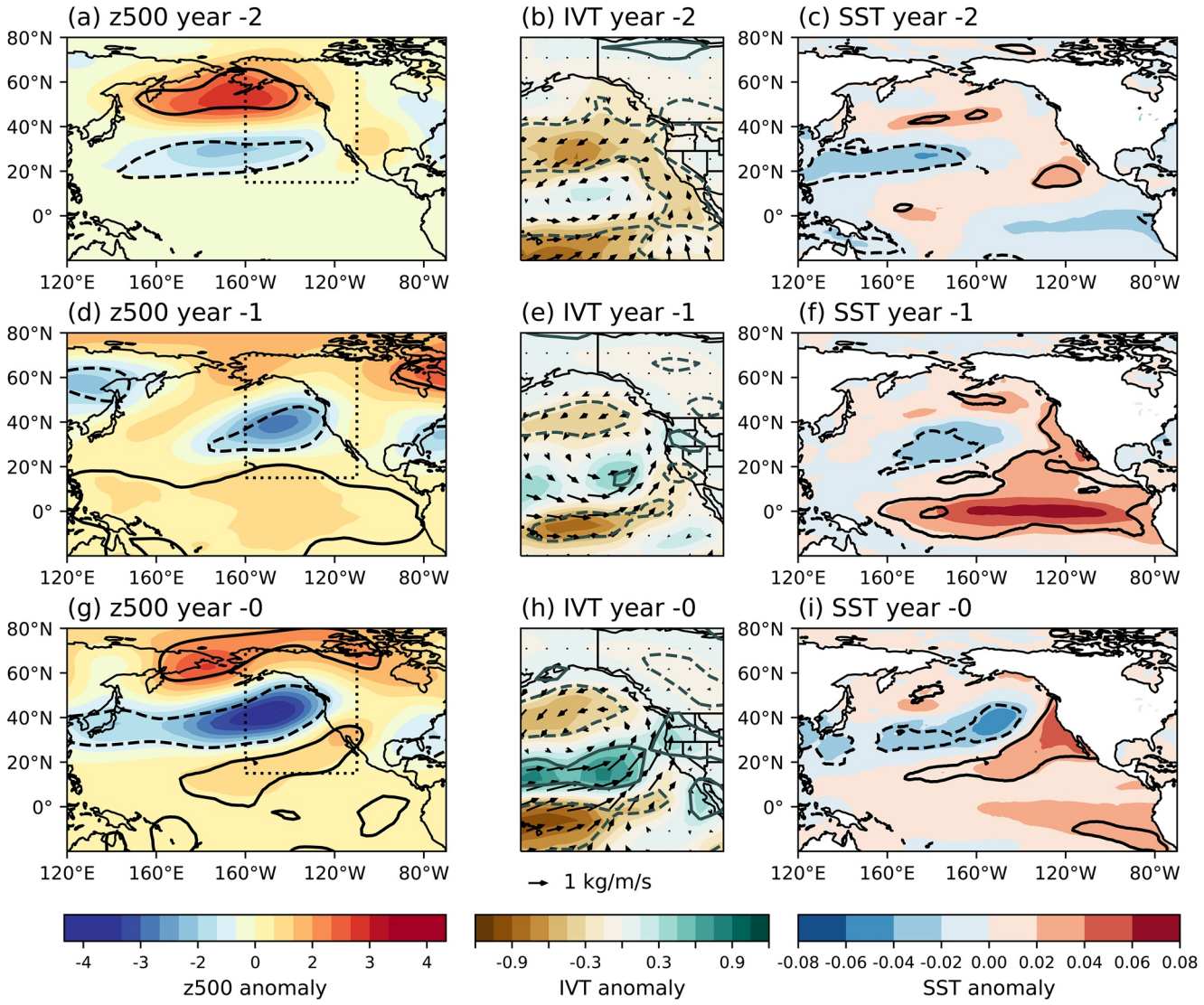

Figure 3. Regression maps of Z500, integrated vapor transport (IVT) and sea surface temperature (SST) anomalies during the wet season at (a–c) -2, (d–f) -1, and (g–i) 0-year leads with the atmospheric river (AR) frequency for 1948–2020. Black contour lines indicate regions where the correlation between the climate variables and AR frequency surpass the 95% confidence interval. The dotted black box in panels a, d and g represents the spatial domain of the IVT in panels b, e and h.

and thus is considered mostly irrelevant for the decadal variability of ARs (Figure 5a). We can also find the NAWD-like Z500 regression pattern with streamflow (Figure S3), but it is not clear in the regressions with AR frequency (Figures 3 and 4). The common feature between each teleconnection and the Z500 regression maps is the Aleutian Low that affects the moisture transport toward Northern California. However, none of the patterns are accurately depicted in the bandpass filtered data (Figures 4a, 4d and 4g). By modulating the position and intensity of the Aleutian low, it appears the NPO and NAWD are important for AR frequency but are not a singular forcing for the quasi-decadal cycle in ARs. It is also possible that the teleconnections could be simultaneously acting to diminish or enhance certain features.

For the oceanic indices, the NPGO and Niño-4 indices exhibit the most pronounced decadal variability (Figure 5b) and the filtered regression maps indicate cyclical behavior. We can find the same pattern with opposite signs of Pacific SST anomalies at 6- and 0-year lead times (Figures 4c and 4i). Consistent with this temporal evolution of SST anomalies, Z500 anomalies also demonstrate the same pattern with opposite signs at 6- and 0-year lead times (Figures 4a and 4g). The SST regressions depict an NPGO-like pattern

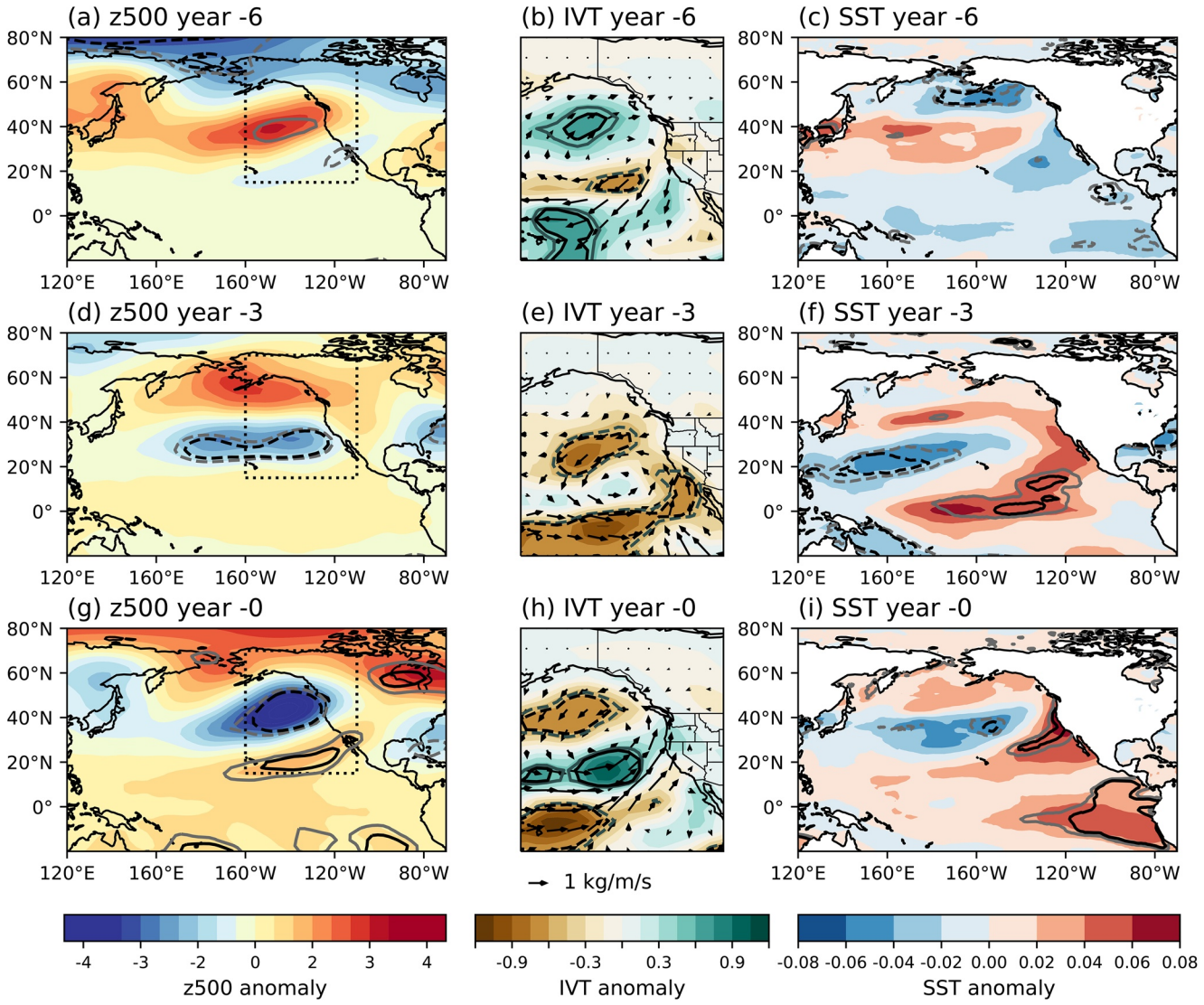

Figure 4. Regression maps of bandpass filtered Z500, IVT, and SST anomalies during the wet season at (a–c) -6, (d–f) -3, and (g–i) 0-year leads with bandpass filtered atmospheric river (AR) frequency for 1948–2020. The dotted rectangle in Figures 4a, 4d and 4g show the domain of Figures 4b, 4e and 4h. The significance testing has been adjusted to account for the reduction in degrees of freedom due to bandpass filtering (72 years of data with a 7-year frequency filter ~8 degrees of freedom). Black and gray contour lines indicate regions where the correlation between the climate variables and AR frequency surpass the 95% and 90% confidence interval respectively.

3 years before peak AR frequency with significant SST anomalies in the equatorial Pacific through 6-, 3-, and 0-year leads. However, the decadal variability of the NPGO (an extra-tropical mode) is tied to central Pacific warming and low-frequency ENSO variability in the tropics (Di Lorenzo et al., 2010, 2015). This indicates the relationship between ARs and the NPGO is largely stimulated by the tropical Pacific.

Observational analysis to this point has shown that the extratropical atmosphere and tropical ocean exhibit an oscillatory behavior on a quasi-decadal scale that is important for IVT transport and Z500 circulation anomalies for Northern California. However, we have not yet isolated the main contributor of quasi-decadal variability. To summarize the series of events linking the ocean to AR frequency, Figure 6 shows the bandpass filtered teleconnection indices as well as their cross correlation with AR frequency. The NAWD shows the strongest concurrent relationship with AR activity between the atmospheric indices–with a negative relationship sensibly indicating that more ARs occur in Northern California during wet seasons with anomalous low-pressure over western North America. The decadal variability of the NPO is slightly out of phase with AR frequency, with the autocorrelation showing the strongest positive relationship 2 years before peak

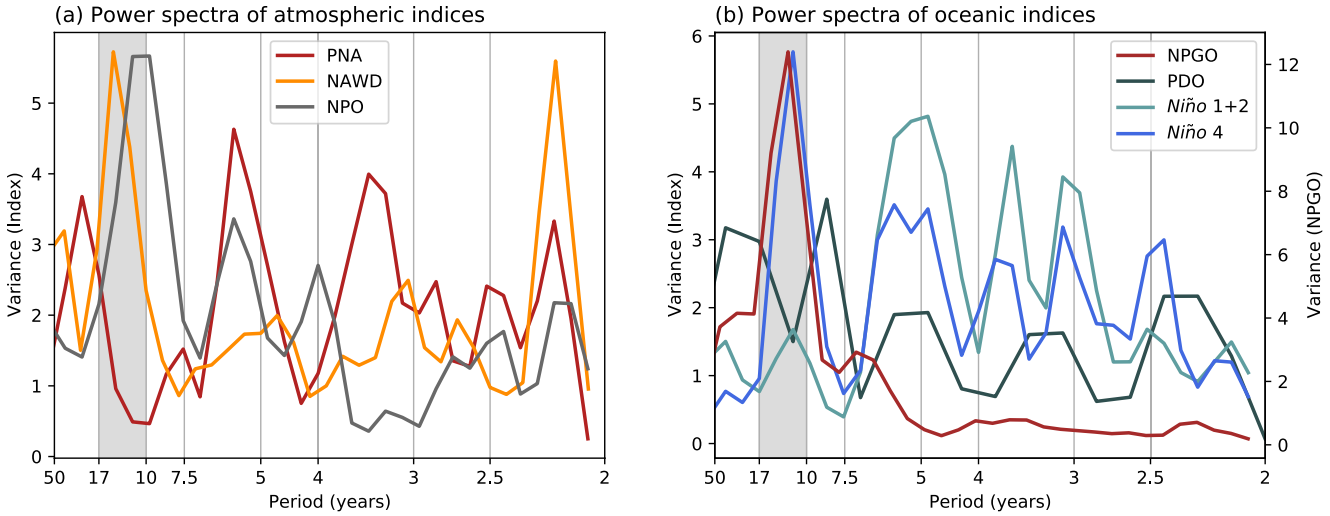

Figure 5. Power spectra of (a) atmospheric and (b) oceanic indices. Atmospheric indices include the Pacific North American (PNA, red), the North American Winter Dipole (NAWD, orange), and the North Pacific Oscillation (NPO, gray) whereas oceanic indices correspond to North Pacific Gyre Oscillation (NPGO, red), Pacific Decadal Oscillation (PDO, dark blue), Niño 1 + 2 (light blue), and Niño 4 (blue) in the 5-month mean from November to the following March. The gray shaded rectangle highlights the period of interest, the quasi-decadal frequency, from 10 to 17 years.

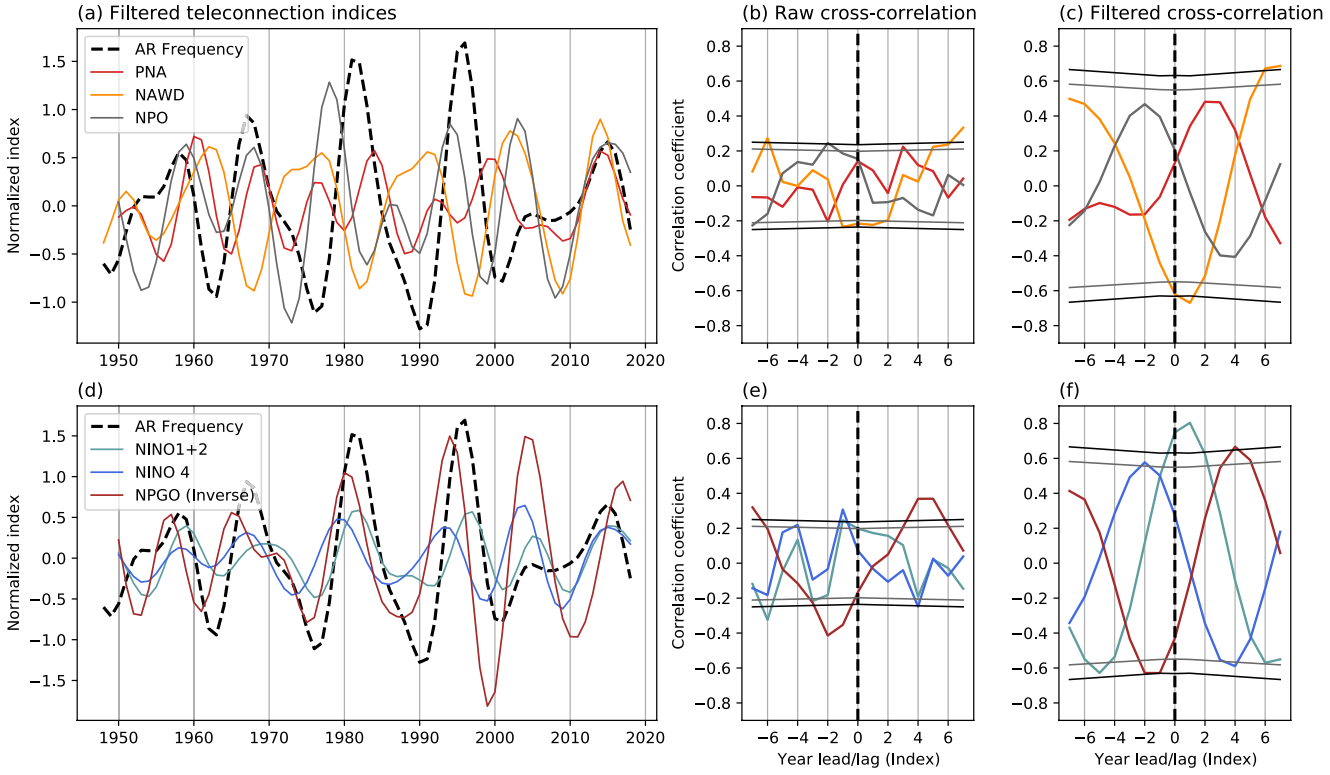

Figure 6. (a) Bandpass filtered atmospheric indices with the bandpass filtered atmospheric river (AR) frequency time series. (b) Cross-correlation between the unfiltered atmospheric indices and the AR frequency timeseries at lead and lag times. (c) Cross-correlation of the bandpass filtered atmospheric indices and AR frequency. The colors in panels b and c match the legend in panel a. (d) Bandpass filtered ocean indices with the bandpass filtered AR frequency time series. (e) Cross-correlation with unfiltered and (f) bandpass filtered ocean indices with AR frequency. The colors in panels e and f match the legend in panels d. The 90% and 95% significance thresholds are represented by the gray and black lines in panels b, c, e, and f—with the threshold changing to match the changing degrees of freedom in comparing the lead/lag relationships.

AR activity. The stronger relationship between the NPO and AR frequency in the unfiltered cross correlation shows that NPO variability is more important for ARs on shorter time scales (also supported in the difference between Figures 3 and 4 regressions at half-phase lead). The PNA shows no leading relationship with ARs and lacks a notable cycle in the autocorrelation, confirming it is not the major forcing. The ocean indices show the same features present in the SST regression maps (Figure 4) with onset central Pacific warming or a positive Niño 4 index leading peak AR frequency by 2–3 years. In line with other literature, the peak NPGO follows central Pacific warming and is a response to the NPO, but these coupled modes of atmospheric and ocean variability exist 1–2 years before peak AR frequency (Di Lorenzo et al., 2010). Additionally, the NAWD has been linked to central Pacific ENSO events at one year lead through anomalous heating of the western north Pacific (Fosu et al., 2020; Wang et al., 2014). These features are detailed in Figure 2 and supported by the cross correlations in Figure 4. Finally, the eastern Pacific warming shown by the Niño 1 + 2 index has a strong and in-phase relationship with AR frequency.

4. Tropical Pacific Modulation of ARs

Section 3 showed that both ocean (Niño 1 + 2 and 4, and the NPGO) and atmospheric variability (the NPO and the NAWD) are significantly related to the quasi-decadal cycle of AR frequency. However, the use of observations makes it difficult to isolate the atmospheric and oceanic forcings. Using the eqPAC of the CESM allows us to better evaluate the cause-and-effect response of AR frequency or extra-tropical atmospheric circulation to the tropical Pacific Ocean alone. To test the importance of the tropical Pacific for quasi-decadal variability in ARs, we created leading regressions of Z500 and SST in the model experiments (i.e., the eqPAC run) with AR frequency. In this model experiment, the simulated atmospheric pattern is the atmospheric response to the equatorial Pacific forcing alone.

To evaluate the model's ability to capture Z500 fields important for AR frequency and support the analysis in NCEP R1, Figure 7 shows a comparison of NCEP R1 Z500 with JRA-55 and the eqPAC Z500 when regressed with AR frequency. In the unfiltered data, the model does not capture the observed extratropical circulation at a 2-year lead. The observations show a clearly defined positive NPO-like pattern, with high-pressure in the central north Pacific around 60°N, and a low-pressure band around 30°N. Other research has shown that the stochastic NPO can force ENSO formation through the seasonal footprinting mechanism, driven by surface heat flux in the north Pacific (Alexander et al., 2010; Anderson, 2003; Vimont et al., 2001, 2003). As an SST assimilated model with the atmosphere free to evolve, stochastic extratropical circulation features like the NPO are not well captured by the model and not represented in the regression maps. This is one plausible explanation for why the 1-year leading regression for the eqPAC run shows a less robust tropical response than the observed data, because the stated extratropical forcing for ENSO would be underrepresented.

Importantly, the 1-year lead and concurrent regressions show that the eqPAC and GLOB runs capture similar circulation features to observations. While the exact orientation and position of high- and low-pressure systems are shifted north by the model, the eqPAC run shows significant modulation of the Aleutian Low by the tropical Pacific (Figure 7). The noted differences between the model and reanalysis Z500 are either from model deficiencies in simulating the extratropical atmosphere or from the inability of the model to capture other forcings important for AR circulation features. The eqPAC also adequately captures the IVT features associated with the Niño 1 + 2 index, though the magnitude of IVT anomalies in the eqPAC is diminished compared to reanalysis (Figure S5). A higher resolution model would likely improve the fidelity of moisture transport and better resolve transient moisture transport (Zhao, 2020). The noted differences between the model and observations are either from model deficiencies in simulating the extratropical atmosphere or from the inability of the eqPAC to simulate other forcings important for extratropical circulation features.

The SST and Z500 regressions from the eqPAC show similar cyclical features to observations, with the most prominent differences noted at the 6-year lead (Figure 8). Generally, the Z500 pattern is shifted to the north when compared to observational Z500. The deepened Aleutian Low with the adjacent subtropical high is still replicated in the regression patterns from the model—generally mirroring the observed relationship (Figures 4d and 4g). The Z500 patterns at the 3-year lead feature an elongated trough in the north Pacific that stretches through North America. The IVT anomalies show that this period is accompanied with below

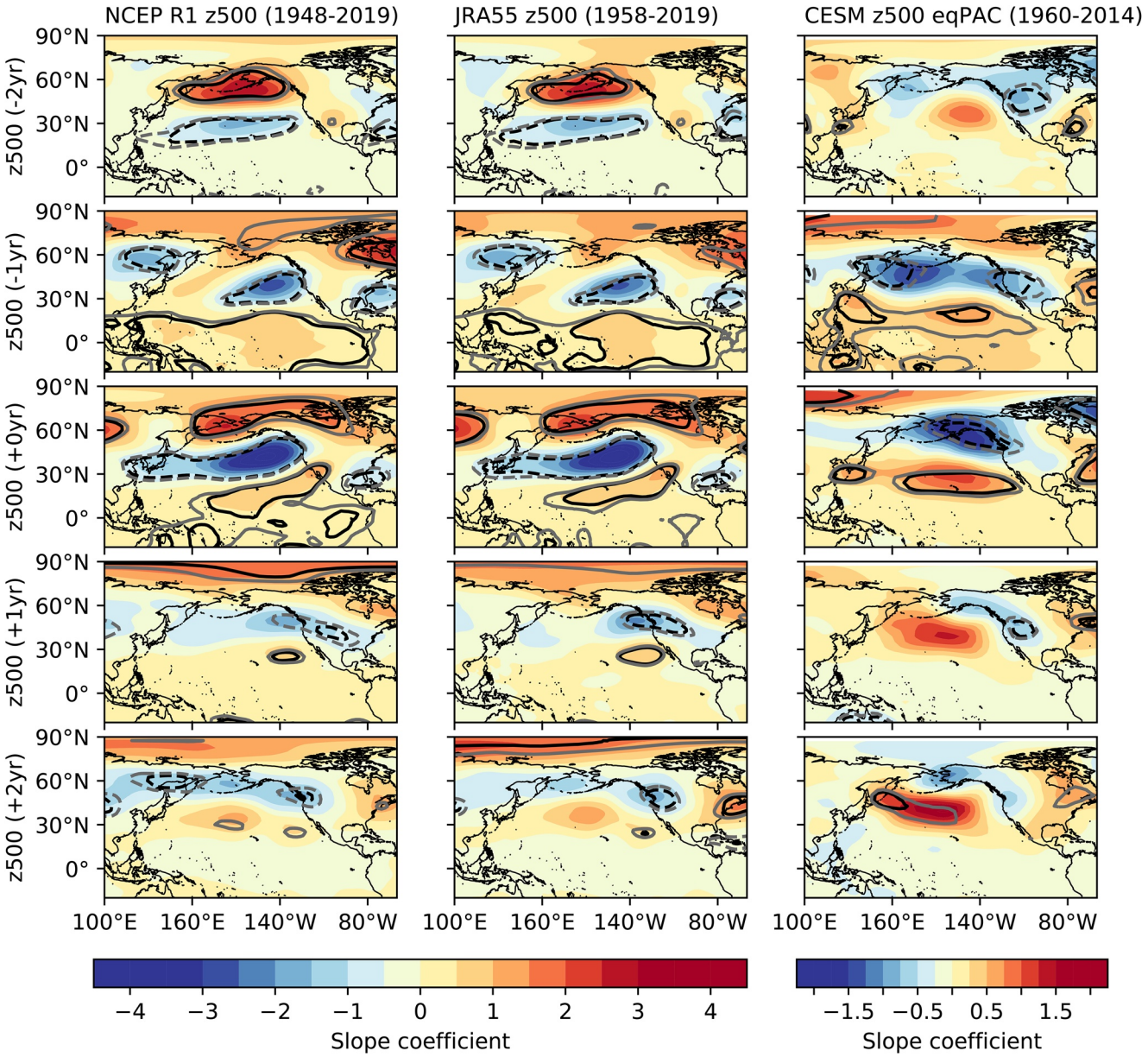

Figure 7. Lead/lag regressions of atmospheric river (AR) frequency with NCEP R1 Z500 (left column). Japanese Meteorological Agency's reanalysis (JRA-55, center column) and the eqPAC z500 (right column). Black and gray contour lines indicate regions where the correlation between Z500 and AR frequency surpass the 95% and 90% confidence interval respectively. The contour levels for the Community Earth System Model (CESM) are half the magnitude of the reanalysis data.

average moisture transport from the tropics (Figure 8e). At 0-year lead, the low pressure in the north Pacific shifts east over the west coast of North America and is accompanied with enhanced IVT anomalies from the tropics (Figures 8g and 8h). The southwest-to-northeast orientation of the frontal zone in the Z500 field in observations at a 0-year lead (Figure 7) is not matched in the eqPAC. Additionally, the SST fields do not show the NPGO-like branch of positive SST anomalies spreading from the central Pacific to the North American coast for the concurrent regression. This suggests that these features are driven by factors other than the tropical Pacific or they might be a response to the meridional pressure dipole noted in the Z500 regressions with observations.

The eqPAC results show that tropical SST and salinity alone have substantial impacts on north Pacific extra-tropical circulation. Without the impact of the extra-tropical atmosphere, central Pacific warming one

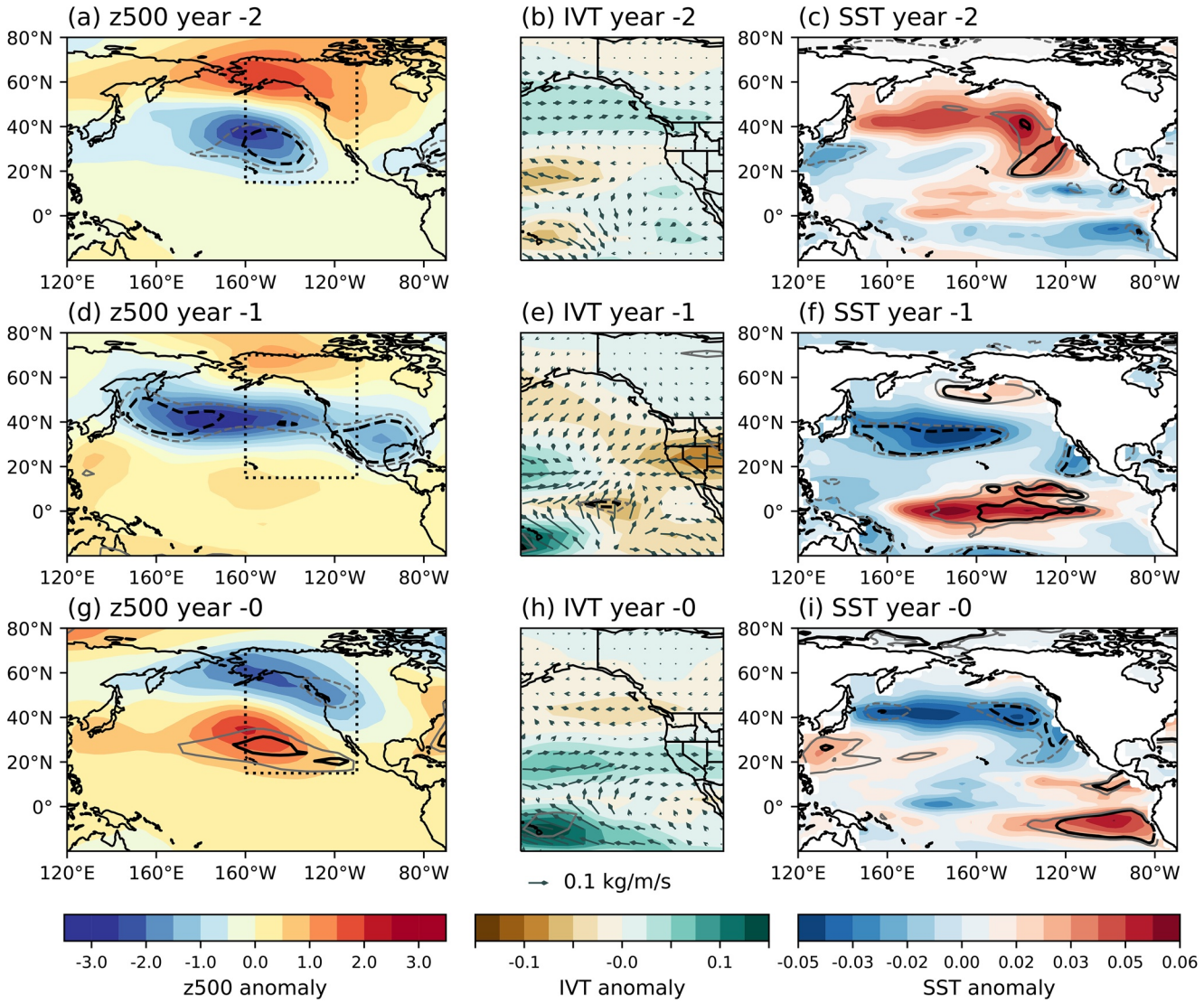

Figure 8. Regression maps of bandpass filtered Z500, integrated vapor transport (IVT), and sea surface temperature (SST) anomalies in the eqPAC during the wet season at (a–c) -6, (d–f) -3, and (g–i) 0-year leads with bandpass filtered atmospheric river (AR) frequency for 1960–2020. The dotted rectangle in panels a, d, and g show the domain of panels b, e, and h. Black and gray contour lines indicate regions where the correlation between Z500 and AR frequency surpass the 95% and 90% confidence interval respectively for 7 degrees of freedom.

year prior to peak AR frequency and eastern Pacific ENSO result in a deepened Aleutian Low with a frontal boundary centered over Northern California (Figure 8). However, the IVT regressions result in features that match the observed circulation but lack the magnitude of the observed IVT and statistical significance. A more accurate simulation for extratropical moisture transport may be achieved with higher model resolution, the assimilation of extratropical SST and the inclusion of SST forcing from the North Pacific and the Atlantic (Chikamoto, Johnson, et al., 2020; Chikamoto, Wang, et al., 2020; Johnson et al., 2020; Zhao, 2020).

5. Conclusions and Discussion

By analyzing seven decades of wet-season AR frequency for Northern California, we show that AR frequency follows a pronounced quasi-decadal cycle with the region's surface and atmospheric moisture variables largely driven by tropical Pacific SST and salinity variability. Observational analysis highlights three important features for AR frequency on quasi-decadal scales:

1. A warming of the Central Pacific that accentuates the Aleutian Low 2–3 years before the peak of quasi-decadal AR frequency
2. A transition from central Pacific warming to eastern Pacific-type ENSO, and the associated eastward shift of the Aleutian Low to a position which facilitates positive IVT anomalies over Northern California
3. A consistent oscillation of the Aleutian Low over 10- to 17-year periods in tandem with the tropical Pacific warming/cooling, modulating AR frequency and wet-season moisture transport.

As the eqPAC run generally captures the extra-tropical response associated with enhanced ARs, we conclude that decadal variability in the tropical Pacific is essential for the frequency of Northern California ARs. However, the CESM-based eqPAC simulations at 3.75° resolution has differences in the Z500 field when compared with observations (Figure 6). The most notable differences are a northward shift in Z500 pressure anomalies and the mildly different orientation in the eqPAC (resulting in a more horizontally oriented frontal zone in the model). There are likely other extratropical factors not considered in this study that are important for the exact orientation and position of the Aleutian Low on the quasi-decadal timescale–potentially explained by internal variability or Arctic climate variability (Chen & Zhai, 2011; Overland et al., 1999).

Interannual climate variability impacts AR characteristics (Guan et al., 2013; Patricola et al., 2020; Ralph et al., 2013) and surface water availability (Jones, 2000; Mo & Higgins, 1998), but the quasi-decadal cycle of ARs (Figures 1b and 1d) is also a fundamental hydrological component for Northern California that has been shown to limit reliable water access for some users (Dettinger, 2016; Morgan et al., 2020). While data limitations do exist and research should continue evaluating low-frequency variability as data records expand, our study supports earlier findings that analysis of low-frequency AR variability is possible with mid-century reanalysis (Gershunov et al., 2017). In a region which has diverse temperature and precipitation responses to ENSO (O'Brien et al., 2019; Patricola et al., 2020), information facilitating climate prediction tools are lacking. Additionally, Northern California has an inherently difficult-to-predict AR-driven precipitation regime (Baggett et al., 2017), but tropical Pacific SST anomalies, specifically central Pacific warming, can serve as precursor patterns for improved decadal prediction of wet-season AR frequency and thus help inform water resource management decisions.

Data Availability Statement

The NCEP reanalysis data used in this study (Kalnay et al., 1996) is publicly available at https://psl.noaa.gov/ while the JRA-55 data are available at https://rda.ucar.edu/. The partial ocean assimilation CESM data used is being placed in an online repository along with the time series of atmospheric rivers for Northern California (https://climate.usu.edu/people/yoshi/res.html).

Acknowledgments
The authors thank Alan Rhoades and another anonymous reviewer for their constructive review. We acknowledge research funding from the U.S. Department of Energy/Office of Science under Award Number DE-SC0016605 and the SERDP project RC20-3056. Y. Chikamoto and S-Y.S. Wang were supported by the Utah Agricultural Experiment Station, Utah State University (approved as journal paper number #9472) and the U.S. Department of Interior, Bureau of Reclamation (R18AC00018, R19AP00149). J. Stuivenvolt-Allen was supported by the National Science Foundation under Grant No. 1633756.

References

Alexander, M. A., Vimont, D. J., Chang, P., & Scott, J. D. (2010). The Impact of extratropical atmospheric variability on ENSO: Testing the seasonal footprinting mechanism using coupled model experiments. *Journal of Climate*, *23*(11), 2885–2901. https://doi.org/10.1175/2010JCLI3205.1

Anderson, B. T. (2003). Tropical Pacific sea-surface temperatures and preceding sea level pressure anomalies in the subtropical North Pacific. *Journal of Geophysical Research*, *108*(D23), 4732. https://doi.org/10.1029/2003JD003805

Baggett, C. F., Barnes, E. A., Maloney, E. D., & Mundhenk, B. D. (2017). Advancing atmospheric river forecasts into subseasonal-to-seasonal time scales. *Geophysical Research Letters*, *44*(14), 7528–7536. https://doi.org/10.1002/2017GL074434

Balmaseda, M. A., Mogensen, K., & Weaver, A. T. (2013). Evaluation of the ECMWF ocean reanalysis system ORAS4. *Quarterly Journal of the Royal Meteorological Society*, *139*(674), 1132–1161. https://doi.org/10.1002/qj.2063

Bao, J.-W., Michelson, S. A., Neiman, P. J., Ralph, F. M., & Wilczak, J. M. (2006). Interpretation of enhanced integrated water vapor bands associated with extratropical cyclones: Their formation and connection to tropical moisture. *Monthly Weather Review*, *134*(4), 1063–1080. https://doi.org/10.1175/MWR3123.1

Chen, Y., & Zhai, P. (2011). Interannual to decadal variability of the winter Aleutian Low intensity during 1900–2004. *Acta Meteorologica Sinica*, *25*(6), 710–724. https://doi.org/10.1007/s13351-011-0602-x

Chikamoto, Y., Johnson, Z. F., Wang, S.-Y. S., McPhaden, M. J., & Mochizuki, T. (2020). El Niño–Southern Oscillation evolution modulated by Atlantic forcing. *Journal of Geophysical Research: Oceans*, *125*(8), e2020JC016318. https://doi.org/10.1029/2020JC016318

Chikamoto, Y., Mochizuki, T., Timmermann, A., Kimoto, M., & Watanabe, M. (2016). Potential tropical Atlantic impacts on Pacific decadal climate trends. *Geophysical Research Letters*, *43*(13), 7143–7151. https://doi.org/10.1002/2016GL069544

Chikamoto, Y., Timmermann, A., Luo, J.-J., Mochizuki, T., Kimoto, M., Watanabe, M., et al. (2015). Skilful multi-year predictions of tropical trans-basin climate variability. *Nature Communications*, *6*(1), 6869. https://doi.org/10.1038/ncomms7869

Chikamoto, Y., Wang, S.-Y. S., Yost, M., Yocom, L., & Gillies, R. R. (2020). Colorado River water supply is predictable on multi-year timescales owing to long-term ocean memory. *Communications Earth & Environment*, *1*(1), 1–11. https://doi.org/10.1038/s43247-020-00027-0
D'Arrigo, R., Cook, E. R., Wilson, R. J., Allan, R., & Mann, M. E. (2005). On the variability of ENSO over the past six centuries. *Geophysical Research Letters*, *32*(3), L03711. https://doi.org/10.1029/2004GL022055
Deser, C., Phillips, A. S., Tomas, R. A., Okumura, Y. M., Alexander, M. A., Capotondi, A., et al. (2011). ENSO and Pacific decadal variability in the community climate system model Version 4. *Journal of Climate*, *25*(8), 2622–2651. https://doi.org/10.1175/JCLI-D-11-00301.1
Dettinger, M. (2011). Climate change, atmospheric rivers, and floods in California – A multimodel analysis of storm frequency and magnitude changes. *JAWRA Journal of the American Water Resources Association*, *47*(3), 514–523. https://doi.org/10.1111/j.1752-1688.2011.00546.x
Dettinger, M. (2016). Historical and future relations between large storms and droughts in California. *San Francisco Estuary and Watershed*, *14*(2), 1–21. https://doi.org/10.15447/sfews.2016v14iss2art1
Dettinger, M., & Cayan, D. R. (2014). Drought and the California Delta–A matter of extremes. *San Francisco Estuary and Watershed Science*, *12*(2), 1–6. https://doi.org/10.15447/sfews.2014v12iss2art4
Dettinger, M. D. (2013). Atmospheric rivers as drought busters on the U.S. west coast. *Journal of Hydrometeorology*, *14*(6), 1721–1732. https://doi.org/10.1175/JHM-D-13-02.1
Di Lorenzo, E., Cobb, K. M., Furtado, J. C., Schneider, N., Anderson, B. T., Bracco, A., et al. (2010). Central Pacific El Niño and decadal climate change in the North Pacific Ocean. *Nature Geoscience*, *3*(11), 762–765. https://doi.org/10.1038/ngeo984
Di Lorenzo, E., Liguori, G., Schneider, N., Furtado, J. C., Anderson, B. T., & Alexander, M. A. (2015). ENSO and meridional modes: A null hypothesis for Pacific climate variability. *Geophysical Research Letters*, *42*(21), 9440–9448. https://doi.org/10.1002/2015GL066281
Ebita, A., Kobayashi, S., Ota, Y., Moriya, M., Kumabe, R., Onogi, K., et al. (2011). The Japanese 55-year reanalysis "JRA-55": An interim report. *Sola*, *7*, 149–152. https://doi.org/10.2151/sola.2011-038
Fan, Y., & Van Den Dool, H. (2004). Climate Prediction Center global monthly soil moisture data set at 0.5° resolution for 1948 to present. *Journal of Geophysical Research*, *109*(D10), D10102. https://doi.org/10.1029/2003JD004345
Fosu, B., He, J., & Wang, S.-Y. S. (2020). The influence of wintertime SST variability in the Western North Pacific on ENSO diversity. *Climate Dynamics*, *54*(7), 3641–3654. https://doi.org/10.1007/s00382-020-05193-7
George, S. S., & Ault, T. R. (2011). Is energetic decadal variability a stable feature of the central Pacific Coast's winter climate? *Journal of Geophysical Research*, *116*(D12), D12102. https://doi.org/10.1029/2010JD015325
Gershunov, A., Shulgina, T., Ralph, F. M., Lavers, D. A., & Rutz, J. J. (2017). Assessing the climate-scale variability of atmospheric rivers affecting western North America. *Geophysical Research Letters*, *44*(15), 7900–7908. https://doi.org/10.1002/2017GL074175
Guan, B., Molotch, N. P., Waliser, D. E., Fetzer, E. J., & Neiman, P. J. (2010). Extreme snowfall events linked to atmospheric rivers and surface air temperature via satellite measurements. *Geophysical Research Letters*, *37*(20), L20401. https://doi.org/10.1029/2010GL044696
Guan, B., Molotch, N. P., Waliser, D. E., Fetzer, E. J., & Neiman, P. J. (2013). The 2010/2011 snow season in California's Sierra Nevada: Role of atmospheric rivers and modes of large-scale variability. *Water Resources Research*, *49*(10), 6731–6743. https://doi.org/10.1002/wrcr.20537
Guan, B., & Waliser, D. E. (2015). Detection of atmospheric rivers: Evaluation and application of an algorithm for global studies. *Journal of Geophysical Research: Atmospheres*, *120*(24), 12514–12535. https://doi.org/10.1002/2015JD024257
Guirguis, K., Gershunov, A., Shulgina, T., Clemesha, R. E. S., & Ralph, F. M. (2019). Atmospheric rivers impacting Northern California and their modulation by a variable climate. *Climate Dynamics*, *52*(11), 6569–6583. https://doi.org/10.1007/s00382-018-4532-5
Gutowski, W. J., Chen, Y., & Ötles, Z. (1997). Atmospheric water vapor transport in NCEP–NCAR reanalyses: Comparison with river discharge in the central United States. *Bulletin of the American Meteorological Society*, *78*(9), 1957–1969. https://doi.org/10.1175/1520-0477(1997)078<1957:AWVTIN>2.0.CO;2
Hersbach, H., Peubey, C., Simmons, A., Berrisford, P., Poli, P., & Dee, D. (2015). ERA-20CM: A twentieth-century atmospheric model ensemble. *Quarterly Journal of the Royal Meteorological Society*, *141*(691), 2350–2375. https://doi.org/10.1002/qj.2528
Higgins, R. W., Schemm, J.-K. E., Shi, W., & Leetmaa, A. (2000). Extreme precipitation events in the western United States related to tropical forcing. *Journal of Climate*, *13*(4), 793–820. https://doi.org/10.1175/1520-0442(2000)013<0793:EPEITW>2.0.CO;2
Ishii, M., Shouji, A., Sugimoto, S., & Matsumoto, T. (2005). Objective analyses of sea-surface temperature and marine meteorological variables for the 20th century using ICOADS and the Kobe collection. *International Journal of Climatology*, *25*(7), 865–879. https://doi.org/10.1002/joc.1169
Johnson, Z. F., Chikamoto, Y., Luo, J.-J., & Mochizuki, T. (2018). Ocean impacts on Australian interannual to decadal precipitation variability. *Climate*, *6*(3), 61. https://doi.org/10.3390/cli6030061
Johnson, Z. F., Chikamoto, Y., Wang, S.-Y. S., McPhaden, M. J., & Mochizuki, T. (2020). Pacific Decadal Oscillation remotely forced by the equatorial Pacific and the Atlantic Oceans. *Climate Dynamics*, *55*(3), 789–811. https://doi.org/10.1007/s00382-020-05295-2
Johnstone, J. A. (2011). A quasi-biennial signal in western US hydroclimate and its global teleconnections. *Climate Dynamics*, *36*(3), 663–680. https://doi.org/10.1007/s00382-010-0755-9
Jones, C. (2000). Occurrence of extreme precipitation events in California and relationships with the Madden–Julian Oscillation. *Journal of Climate*, *13*(20), 3576–3587. https://doi.org/10.1175/1520-0442(2000)013<3576:OOEPEI>2.0.CO;2
Kalnay, E., Kanamitsu, M., Kistler, R., Collins, W., Deaven, D., Gandin, L., et al. (1996). The NCEP/NCAR 40-year reanalysis project. *Bulletin of the American Meteorological Society*, *77*(3), 437–471. https://doi.org/10.1175/1520-0477(1996)077<0437:TNYRP>2.0.CO;2
Kim, H.-M., & Alexander, M. A. (2015). ENSO's modulation of water vapor transport over the Pacific–North American region. *Journal of Climate*, *28*(9), 3846–3856. https://doi.org/10.1175/JCLI-D-14-00725.1
Knutson, T. R., & Manabe, S. (1998). Model assessment of decadal variability and trends in the Tropical Pacific Ocean. *Journal of Climate*, *11*(9), 2273–2296. https://doi.org/10.1175/1520-0442(1998)011<2273:MAODVA>2.0.CO;2
Liu, X., Ren, X., & Yang, X.-Q. (2016). Decadal changes in multiscale water vapor transport and atmospheric river associated with the Pacific Decadal Oscillation and the North Pacific Gyre Oscillation. *Journal of Hydrometeorology*, *17*(1), 273–285. https://doi.org/10.1175/JHM-D-14-0195.1
Lorenzo, E. D., Schneider, N., Cobb, K. M., Franks, P. J. S., Chhak, K., Miller, A. J., et al. (2008). North Pacific Gyre Oscillation links ocean climate and ecosystem change. *Geophysical Research Letters*, *35*(8), L08607. https://doi.org/10.1029/2007GL032838
MacDonald, G. M., & Case, R. A. (2005). Variations in the Pacific Decadal Oscillation over the past millennium. *Geophysical Research Letters*, *32*(8), L08703. https://doi.org/10.1029/2005GL022478
Mantua, N. J., Hare, S. R., Zhang, Y., Wallace, J. M., & Francis, R. C. (1997). A Pacific Interdecadal Climate Oscillation with impacts on Salmon production. *Bulletin of the American Meteorological Society*, *78*(6), 1069–1079. https://doi.org/10.1175/1520-0477(1997)078<1069:APICOW>2.0.CO;2

Mo, K. C., & Higgins, R. W. (1998). Tropical influences on California precipitation. *Journal of Climate*, *11*(3), 412–430. https://doi.org/10.1175/1520-0442(1998)011<0412:TIOCP>2.0.CO;2

Morgan, B., Spangler, K., Stuivenvolt Allen, J., Morrisett, C. N., Brunson, M. W., Wang, S.-Y. S., & Huntly, N. (2020). Water availability for Cannabis in Northern California: Intersections of climate, policy, and public discourse. *Water*, *13*(1), 5. https://doi.org/10.3390/w13010005

Mundhenk, B. D., Barnes, E. A., Maloney, E. D., & Baggett, C. F. (2018). Skillful empirical subseasonal prediction of landfalling atmospheric river activity using the Madden–Julian oscillation and quasi-biennial oscillation. *Npj Climate and Atmospheric Science*, *1*(1), 1–7. https://doi.org/10.1038/s41612-017-0008-2

Newman, M., Alexander, M. A., Ault, T. R., Cobb, K. M., Deser, C., Di Lorenzo, E., et al. (2016). The Pacific Decadal Oscillation, revisited. *Journal of Climate*, *29*(12), 4399–4427. https://doi.org/10.1175/JCLI-D-15-0508.1

O'Brien, J. P., O'Brien, T. A., Patricola, C. M., & Wang, S.-Y. S. (2019). Metrics for understanding large-scale controls of multivariate temperature and precipitation variability. *Climate Dynamics*, *53*(7), 3805–3823. https://doi.org/10.1007/s00382-019-04749-6

Overland, J. E., Adams, J. M., & Bond, N. A. (1999). Decadal variability of the Aleutian Low and its relation to high-latitude circulation. *Journal of Climate*, *12*(5), 1542–1548. https://doi.org/10.1175/1520-0442(1999)012<1542:DVOTAL>2.0.CO;2

Patricola, C. M., O'Brien, J. P., Risser, M. D., Rhoades, A. M., O'Brien, T. A., Ullrich, P. A., et al. (2020). Maximizing ENSO as a source of western US hydroclimate predictability. *Climate Dynamics*, *54*(1), 351–372. https://doi.org/10.1007/s00382-019-05004-8

Payne, A. E., & Magnusdottir, G. (2014). Dynamics of Landfalling Atmospheric Rivers over the North Pacific in 30 Years of MERRA Reanalysis. *Journal of Climate*, *27*(18), 7133–7150. https://doi.org/10.1175/JCLI-D-14-00034.1

Purich, A., England, M. H., Cai, W., Chikamoto, Y., Timmermann, A., Fyfe, J. C., et al. (2016). Tropical Pacific SST drivers of recent Antarctic Sea ice trends. *Journal of Climate*, *29*(24), 8931–8948. https://doi.org/10.1175/JCLI-D-16-0440.1

Ralph, F. M., Coleman, T., Neiman, P. J., Zamora, R. J., & Dettinger, M. D. (2013). Observed impacts of duration and seasonality of atmospheric-river landfalls on soil moisture and runoff in Coastal Northern California. *Journal of Hydrometeorology*, *14*, 443, 459. https://doi.org/10.1175/JHM-D-12-076.1

Rodgers, K. B., Friederichs, P., & Latif, M. (2004). Tropical Pacific decadal variability and its relation to decadal modulations of ENSO. *Journal of Climate*, *17*(19), 3761–3774. https://doi.org/10.1175/1520-0442(2004)017<3761:TPDVAI>2.0.CO;2

Rutz, J. J., Shields, C. A., Lora, J. M., Payne, A. E., Guan, B., Ullrich, P., et al. (2019). The Atmospheric River Tracking Method Intercomparison Project (ARTMIP): Quantifying uncertainties in atmospheric river climatology. *Journal of Geophysical Research: Atmospheres*, *124*(24), 13777–13802. https://doi.org/10.1029/2019JD030936

Ryoo, J.-M., Kaspi, Y., Waugh, D. W., Kiladis, G. N., Waliser, D. E., Fetzer, E. J., & Kim, J. (2013). Impact of Rossby wave breaking on U.S. west coast winter precipitation during ENSO events. *Journal of Climate*, *26*(17), 6360–6382. https://doi.org/10.1175/JCLI-D-12-00297.1

Schneider, U., Becker, A., Finger, P., Meyer-Christoffer, A., Ziese, M., & Rudolf, B. (2014). GPCC's new land surface precipitation climatology based on quality-controlled in situ data and its role in quantifying the global water cycle. *Theoretical and Applied Climatology*, *115*(1), 15–40. https://doi.org/10.1007/s00704-013-0860-x

Shields, C. A., Bailey, D. A., Danabasoglu, G., Jochum, M., Kiehl, J. T., Levis, S., & Park, S. (2012). The low-resolution CCSM4. *Journal of Climate*, *25*(12), 3993–4014. https://doi.org/10.1175/JCLI-D-11-00260.1

Shields, C. A., Rutz, J. J., Leung, L.-Y., Ralph, F. M., Wehner, M., Kawzenuk, B., et al. (2018). Atmospheric River Tracking Method Intercomparison Project (ARTMIP): Project goals and experimental design. *Geoscientific Model Development*, *11*(6), 2455–2474. https://doi.org/10.5194/gmd-11-2455-2018

Slivinski, L. C., Compo, G. P., Whitaker, J. S., Sardeshmukh, P. D., Giese, B. S., McColl, C., et al. (2019). Towards a more reliable historical reanalysis: Improvements for version 3 of the Twentieth Century Reanalysis system. *Quarterly Journal of the Royal Meteorological Society*, *145*(724), 2876–2908. https://doi.org/10.1002/qj.3598

Tan, Y., Zwiers, F., Yang, S., Li, C., & Deng, K. (2020). The role of circulation and its changes in present and future atmospheric rivers over western North America. *Journal of Climate*, *33*(4), 1261–1281. https://doi.org/10.1175/JCLI-D-19-0134.1

Timmermann, A., An, S.-I., Kug, J.-S., Jin, F.-F., Cai, W., Capotondi, A., et al. (2018). El Niño–Southern Oscillation complexity. *Nature*, *559*(7715), 535–545. https://doi.org/10.1038/s41586-018-0252-6

Vimont, D. J., Battisti, D. S., & Hirst, A. C. (2001). Footprinting: A seasonal connection between the tropics and mid-latitudes. *Geophysical Research Letters*, *28*(20), 3923–3926. https://doi.org/10.1029/2001GL013435

Vimont, D. J., Wallace, J. M., & Battisti, D. S. (2003). The seasonal footprinting mechanism in the Pacific: Implications for ENSO. *Journal of Climate*, *16*(16), 2668–2675. https://doi.org/10.1175/1520-0442(2003)016<2668:TSFMIT>2.0.CO;2

Wang, S. Y., Gillies, R. R., Hipps, L. E., & Jin, J. (2011). A transition-phase teleconnection of the Pacific quasi-decadal oscillation. *Climate Dynamics*, *36*, 681–693. https://doi.org/10.1007/s00382-009-0722-5

Wang, S.-Y., Gillies, R. R., Jin, J., & Hipps, L. E. (2009). Recent rainfall cycle in the intermountain region as a quadrature amplitude modulation from the Pacific decadal oscillation. *Geophysical Research Letters*, *36*(2), L02705. https://doi.org/10.1029/2008GL036329

Wang, S.-Y., Hipps, L., Gillies, R. R., & Yoon, J.-H. (2014). Probable causes of the abnormal ridge accompanying the 2013–2014 California drought: ENSO precursor and anthropogenic warming footprint. *Geophysical Research Letters*, *41*(9), 3220–3226. https://doi.org/10.1002/2014GL059748

Wang, S.-Y. S., Huang, W.-R., & Yoon, J.-H. (2015). The North American winter 'dipole' and extremes activity: A CMIP5 assessment. *Atmospheric Science Letters*, *16*(3), 338–345. https://doi.org/10.1002/asl2.565

Wang, S.-Y. S., Yoon, J.-H., Becker, E., & Gillies, R. (2017). California from drought to deluge. *Nature Climate Change*, *7*, 465–468. https://doi.org/10.1038/nclimate3330

World Meteorological Organization. (2017). *WMO guidelines on the calculation of climate normals*. WMO.

Wu, L., Liu, Z., Gallimore, R., Jacob, R., Lee, D., & Zhong, Y. (2003). Pacific decadal variability: The tropical Pacific Mode and the North Pacific Mode. *Journal of Climate*, *16*(8), 1101–1120. https://doi.org/10.1175/1520-0442(2003)16<1101:PDVTTP>2.0.CO;2

Wu, S., Liu, Z., Zhang, R., & Delworth, T. L. (2011). On the observed relationship between the Pacific Decadal Oscillation and the Atlantic Multi-decadal Oscillation. *Journal of Oceanography*, *67*(1), 27–35. https://doi.org/10.1007/s10872-011-0003-x

Yeh, S.-W., & Kirtman, B. P. (2005). Pacific decadal variability and decadal ENSO amplitude modulation. *Geophysical Research Letters*, *32*(5), L05703. https://doi.org/10.1029/2004GL021731

Zhao, M. (2020). Simulations of atmospheric rivers, their variability, and response to global warming using GFDL's new high-resolution general circulation model. *Journal of Climate*, *33*(23), 10287–10303. https://doi.org/10.1175/JCLI-D-20-0241.1